The Planetary Science Journal, 3:118 (12pp), 2022 May https://doi.org/10.3847/PSJ/ac686c

Dynamical Evolution of Ejecta from the DART Impact on Dimorphos

Alessandro Rossi[1], Francesco Marzari[2], John Robert Brucato[3], Vincenzo Della Corte[4], Elisabetta Dotto[5], Simone Ieva[5], Stavro Lambrov Ivanovski[6], Alice Lucchetti[7], Elena Mazzotta Epifani[5], Maurizio Pajola[7], Giovanni Poggiali[3], and Angelo Zinzi[8]
The LICIACube Team

[1] Istituto di Fisica Applicata "Nello Carrara" (IFAC-CNR), Sesto Fiorentino 50019, Italy; a.rossi@ifac.cnr.it
[2] University of Padova, Padova, Italy
[3] INAF Osservatorio Astrofisico di Arcetri, Firenze, Italy
[4] INAF Istituto di Astrofisico e Planetologia Spaziali, Roma, Italy
[5] INAF Osservatorio Astronomico di Roma, Roma, Italy
[6] INAF Osservatorio Astronomico di Trieste, Trieste, Italy
[7] INAF Osservatorio Astronomico di Padova, Padova, Italy
[8] ASI Agenzia Spaziale Italiana, Roma, Italy
Received 2022 January 28; revised 2022 April 12; accepted 2022 April 15; published 2022 May 25

Abstract

The DART spacecraft will impact Dimorphos (the secondary body of the Didymos binary asteroid) to test the kinetic impactor deflection method against possibly hazardous near-Earth asteroids. The DART impact ejecta plume, and possibly the impact crater, will be imaged by the LICIACube spacecraft, hosted as a piggyback and released by DART just before the impact, and then, several years later, by the Hera probe. To exploit the wealth of data obtained and understand the physics of the whole impact experiment, it is of paramount importance to properly model the dynamics of the binary system pre- and postimpact and the dynamics of the particles ejected from the impact crater. A model was developed to simulate the evolution of the ejecta particles created during the impact in order to first interpret the LICIACube images and then test the survival of particles on long intervals of time that might be detected by the Hera mission either as individual bodies or as parts of rings. The dynamical evolution of the particles is simulated over different timescales to highlight the most important perturbations and their relative importance. The ejecta dynamics turns out to be highly chaotic due to repeated close encounters with the two asteroids. However, we find that some ejecta survive in the binary orbital environment for timescales comparable to the Hera arrival time. The effects of the particles reimpacting against either one of the components is also analyzed to estimate the amount of momentum transfer to the target bodies.

Unified Astronomy Thesaurus concepts: Near-Earth objects (1092)

1. Introduction

The Asteroid Impact Deflection Assessment (AIDA) is an international cooperation whose main objective is to develop technologies to deflect an asteroid if it were on a collision course with Earth. First, the NASA-APL Double Asteroid Redirection Test (DART) spacecraft (Rivkin et al. 2021) will impact at a speed of about 6 km s^{-1} on Dimorphos, the secondary member of an S-type near-Earth binary asteroid of the Apollo–Amor group whose main body is (65803) Didymos. The impact, crater formation, and debris ejection will be observed in real time from the Italian Space Agency probe LICIACube, a cubesat released 10 days before the impact (Dotto et al. 2021), while ground observatories will measure, in the following weeks and months, the change in the rotation period of Dimorphos around Didymos. The European contribution to AIDA is the European Space Agency spacecraft Hera, which will be launched 2 yr later and rendezvous with the binary asteroid in 2026 to perform close-up measurements of the crater excavated by DART to gain insights into the physical and mineralogical characteristics of the asteroid and evaluate the deflection efficiency (Michel et al. 2022).

The debris cloud lifted after the impact will leave the surface of Dimorphos and dynamically evolve in the complex gravity field of the binary asteroid also affected by the Sun tidal force and solar radiation pressure (SRP). All of these forces open different evolutionary channels for the ejecta fragments. In the short term, impact on either Dimorphos or Didymos or escape from the system on hyperbolic trajectories are the dominant behaviors (Yu & Michel 2018). In the long term, injection on temporary orbits may occur either around the two bodies or in circumbinary orbits. The formation of one or more rings after the DART impact is an intriguing possibility, since other minor bodies, like the two Centaurs Chariklo and Chiron (Braga-Ribas et al. 2014; Ortiz et al. 2015; Ruprecht et al. 2015) and the TNO Haumea (Ortiz et al. 2017), are known to have a ring system detected by stellar occultation. One possible explanation for the formation of their rings is exactly a collision with a smaller body, asteroid, or comet, which blasted debris into orbits where they were subsequently stabilized by mutual collisions or gravitational perturbations of satellites of the central body.

The presence of a satellite can be constructive if it helps in stabilizing the orbits of the ejecta fragments, but it can also jeopardize the long-term survival of a ring if its gravitational perturbations are too strong, like, for example, in the presence

of Kozai–Lidov configurations (Marzari 2020). In the case of the Didymos–Dimorphos pair, the mass ratio between the two bodies is large, leading to a configuration that is closer to a binary asteroid than an asteroid with a satellite. As a consequence, the irregular gravity field of the binary configuration may prevent the formation of long-lasting ring systems. For the safety of the Hera mission, however, even a temporary ring may pose a significant threat due to potential collisions with debris fragments still in orbit in the vicinity of the asteroids.

The evolution of the debris fragments is interesting even from a purely scientific perspective due to the complexity of the dynamics driven by four different forces whose strength may change depending on time and the initial conditions of the debris cloud. We focus in this paper on the possible injection of some ejecta from the surface of Dimorphos into temporary or long-term stable orbits. Even temporary stable orbits are interesting, since they may be detected by Hera, and the source of their chaoticity needs to be explored. From a statistical point of view, it would be desirable to also evaluate the fraction of debris particles ending in the different dynamical channels in order to map the phase space. This investigation is left for future work. Additional questions concern the particle size for which radiation pressure becomes an important perturbation and the contribution of the solar tide to the stability of the debris trajectories. Finally, it is of interest to evaluate the role of the initial conditions of the debris fragments just after the impact to determine the subsequent evolution of the debris. If Hera detects some particles in orbit in the system, can we compute back in time its initial ejection velocity vector? If so, we might have important clues to the physics of the impact.

To answer these questions, we have developed a computer code, dubbed LICEI (LICIACube Ejecta Integrator), to model the dynamical evolution of the debris after its ejection from Dimorphos. We account for the irregular gravity field of both Dimorphos and Didymos and include the effects of radiation pressure and solar tide. We consider different particle sizes and evolve a large number of trajectories to have a hint of the statistical behavior of the debris cloud.

In Section 2, a brief introduction to the dynamical model implemented in our code is given. Then, in Section 2.5, a sensitivity analysis for some of the models and assumptions adopted in the simulations is presented. In Section 3.1, a sample of the short-term analysis of the plume is presented. In Sections 3.2–3.4, the chaotic nature of the ejecta trajectories is introduced, and the analysis of long-term surviving particles is presented. In Section 3.5, the influence on the system dynamics of particles reimpacting the two asteroids is analyzed. Finally, the conclusions are listed in Section 4.

2. The Dynamical Model

To investigate the dynamics of the ejecta fragments, once they leave the surface of Dimorphos, we numerically integrate their trajectories. During their evolution, the fragments may have frequent close encounters with the two components of the binary, making their orbits highly chaotic. The 15th-order Radau numerical integrator (Everhart 1985), which has a variable step size and is very accurate in modeling close approaches, is very well suited to handle this problem.

Our numerical model includes (1) the gravity field of both Didymos and Dimorphos, (2) the solar gravity computed as an external perturbation, and (3) the radiation pressure force (including shadowing), where variable shapes and rotation for the particles can be adopted. Collisions between the ejecta particles themselves are currently not considered in the model.

2.1. The Gravitational Force

The gravitational attraction of the two massive bodies on the massless particles is computed either with an analytical approach based on the MacCullagh formula (Murray & Dermott 2000) or with a polyhedral approach (Werner 1994; Werner & Scheeres 1997).

The MacCullagh formula allows a fast computation of the potential through the equation

$$V = -\frac{GM}{r} - \frac{G(A + B + C - 3I)}{2r^3}, \tag{1}$$

with the term I given by Murray & Dermott (2000),

$$I = \frac{(Ax^2 + By^2 + Cz^2)}{r^2}, \tag{2}$$

where A, B, and C are the inertia moments of the body along the principal axes. For a triaxial ellipsoid, the inertia moments are related to the principal semiaxes a, b, and c through the equations

$$A = \frac{4}{15}\pi\rho abc(b^2 + c^2)$$
$$B = \frac{4}{15}\pi\rho abc(a^2 + c^2)$$
$$C = \frac{4}{15}\pi\rho abc(a^2 + b^2),$$

where ρ is the density of the body. The formula for the potential is derived for asymmetric bodies assuming that the ratio between the distance r_i of each mass element of the attracting body with respect to its barycenter and the distance of the attracted body r is a small number so that the series expansion can be truncated to the second order in r_i/r.

The polyhedral approach is based on the fact that any body of arbitrary shape can be approximated with a set of polyhedrons having a variable number of faces. According to Werner (1994), it is possible to compute with analytical formulae the gravitational potential of a homogeneous polyhedron having triangular faces. It is given as

$$V = \frac{1}{2}G\rho\sum_{e\in \text{edges}} \boldsymbol{r}_e \cdot \boldsymbol{E}_e \cdot \boldsymbol{r}_e \cdot L_e - \frac{1}{2}G\rho \times \sum_{f\in \text{faces}} \boldsymbol{r}_f \cdot \boldsymbol{F}_f \cdot \boldsymbol{r}_f \cdot \omega_f, \tag{3}$$

where the first sum is over all edges of the polyhedrons, while the second is over all faces. The vector $\boldsymbol{r}_e$ goes from any position in the gravity fields to each edge, $\boldsymbol{E}_e$ is a dyad defined in terms of the face and edge normal vectors associated with each edge, L_e is a logarithmic term expressing the potential of a 1D straight wire, $\boldsymbol{F}_f$ is a dyad defined for each face as the outer product of the face unit normal vector with itself, and, finally, ω_f is the signed solid angle subtended by a face when viewed from the field point. Once the shape model of an asteroid is known, a polyhedron model can be built to compute the gravity field of the object. As shown in Rossi et al. (1999), the polyhedral approach is the best model (once compared to

analytical or mascons models) to compute the gravity close to the surface of an irregular body.

In both approaches, MacCullagh's and polyhedral, the rotation of each of the two massive bodies around any direction can be accounted for.

2.2. Solar Radiation Pressure

The SRP force is computed as

$$\boldsymbol{F} = \frac{SA}{c} Q_{PR}, \tag{4}$$

where S is the solar radiation flux density at the heliocentric distance of the body, A is the grains' geometrical cross section, and Q_{PR} is a dimensionless coefficient determining the amount of radiation that is either reflected or absorbed and reemitted (Burns et al. 1979). We neglect the Poynting–Robertson drag, since the timescales of interest for our study are too short for it to be relevant (see also Yu et al. 2017).

Since the radiation pressure is linearly proportional to the cross section of the ejecta fragments, we consider different configurations. We assume that the ejecta particles are ellipsoids, and either we read their shape and dimensions from an input file, or we draw them from the outcome of impact experiments (Giblin et al. 2004).

In the radiation force, the cross section A is the relevant parameter and, for a rotating ellipsoid, A can change following the rotation state of the particle. For this reason, we consider different possible rotation states that lead to different A values during the integration:

1. regular rotation around the principal axis with a fixed assigned period;
2. regular rotation around the principal axis with a period extracted, for each particle, from a Maxwellian distribution; and
3. random tumbling simulated by randomly changing the aspect area A of the given ellipsoid from $A_{\min}$ to $A_{\max}$ at each time step.

Eclipses by both asteroids are taken into account, assuming a cylindrical shape for the shadow. Penumbra effects are disregarded, taking into account their limited relative importance, the stability of the integrator even in the presence of step functions when the SRP is turned on and off, and the absence of an atmosphere, which makes the penumbra effects less pronounced (Milani et al. 1987). The position of the Sun is analytically computed from a reference orbit.

2.3. The Choice of the Reference Frame

Since the fragments are ejected from the surface of Dimorphos after the impact, the natural choice of initial reference frame is one centered on Dimorphos with the inclusion of the proper indirect term. The final trajectories are then moved to a reference frame centered on Didymos for a detailed investigation of their evolution.

The impacts against the primary and secondary ellipsoidal bodies are recorded in both the MacCullagh and polyhedral models, while bodies whose distance exceeds twice the Hill radius of Didymos are considered to have escaped from the system. In case of reimpacts against the two asteroids, the location and velocity vectors of the events are recorded.

2.4. Initial Conditions for the Ejecta

Many numerical simulations of the DART impact have been performed in recent years analyzing the effect of different projectile and target characteristics. (e.g., Stickle et al. 2020; Raducan et al. 2021, 2022; Zhang et al. 2021). Initially, for this study, the results of iSALE-2D simulations of head-on impacts of an aluminum projectile on a basalt target with an internal friction coefficient of 0.6, cohesive strength of 10 KPa, and porosity of 20% were used (provided by Raducan et al. 2019). However, it turned out that in such a high-cohesion regime, the ejecta, in order to detach from the surface, have high ejection velocities, usually significantly in excess of the body escape velocity ($\sim$10 cm s^{-1} for Dimorphos). The original distribution of the ejection velocity is shown in Figure 1. Since we are interested in analyzing the medium-term evolution of particles within the binary system, in our modeling in some cases, we used the left (slow) tail of the velocity distribution shown in Figure 1 up to 20 cm s^{-1}, while in other simulations, we kept the original velocity unit vector from the iSALE simulation but rescaled its modulus in order to consider lower ejection speeds that may be the outcome of impacts on weaker bodies. Moreover, in the simulations of Section 3, as detailed in the text, the ejection velocity was simply put equal to a given value ($\sim$7 cm s^{-1}) in order to have the same conditions for all of the tests under exam. The influence of the target composition on the escape velocities may be part of future work stemming from different impact simulation data.

2.5. Sensitivity Analysis

Starting from the overall model described in the previous section, an analysis of the sensitivity of the results from some of the main parameters and assumptions was performed. A similar analysis, also covering other effects mentioned in Section 2 but not considered in the present work, can be found in Yu et al. (2017) and Yu & Michel (2018). At difference from the model described in these two papers, here we concentrate on the effects, also on longer timescales, of the different modeling of the gravity fields of the asteroids and a more refined modeling of the SRP effects, considering ellipsoidal rotating particles, with respect to the simple spherical approximation considered in previous works.

2.5.1. Comparison between the Analytical and Polyhedron Approaches

As shown, e.g., in Rossi et al. (1999), the polyhedral approach is more accurate close to the surface compared to other approaches (mascons or analytical developments). However, its downside is that it is very CPU demanding compared to the other methods. In our case, a possible approach is to use the polyhedron model when the particles leave the surface, and, once they are reasonably far from the body, we switch to the analytical MacCullagh potential to continue the numerical integration over a long time span. On the other hand, as will be shown in the following sections, the dynamics of the particles ejected from the surface of Dimorphos is highly chaotic due to the repeated encounters with the asteroid pair. As a consequence, even if we achieve a high resolution close to the surface, this may not be really relevant in determining the long-term evolution of the ejecta.

If we adopt a patched approach, where we use the polyhedron model close to the surface and the MacCullagh

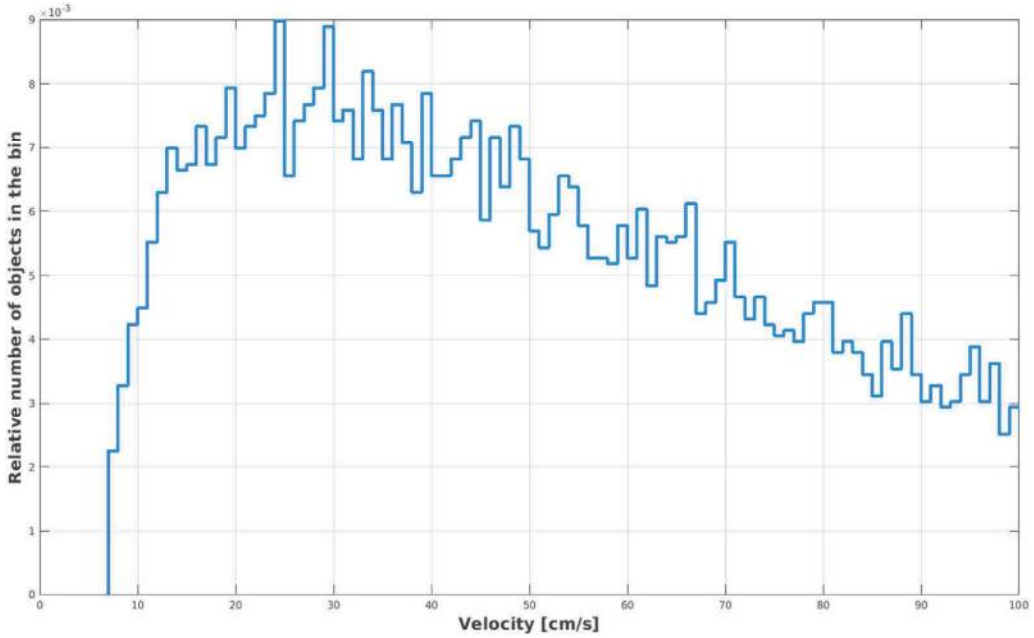

Figure 1. Original velocity distribution for the considered impact simulation from Raducan et al. (2019), truncated at 1 m s $^{-1}$. The histogram shows the number of objects relative to the total of 11,593 particles within each bin of 1 cm s $^{-1}$.

potential far from the surface of Dimorphos, the solutions are very close to the polyhedron-only model. The actual threshold value (either in time or in distance from the central body) for the switch between the two computational methods is an input parameter to the code. In Figure 2, we compare the patched solution, where we switch to the MacCullagh potential approximately 500 m above Dimorphos's surface, to the full polyhedron model. We notice that the two solutions are almost indistinguishable from each other in spite of the high chaotic nature of the solution. This is a significant advantage because the numerical integration with MacCullagh's potential is much faster and can be used to compute the evolution of a larger number of particles. In addition, the polyhedron model requires a lot more numerical computations to derive the potential, leading to a surge in the rounding-off error at each time step, while this does not happen in the MacCullagh approach.

2.5.2. The Influence of the SRP

The SRP for small ejecta may become a dominant force and significantly perturb their dynamical evolution. As pointed out in Rossi & Fulchignoni (2007), for small particles, the SRP can become dominant over the gravitational attraction at a few tens of radii of distance from the central body. As an example, considering the order-of-magnitude equations in Section 2.1 of Rossi & Fulchignoni (2007), assuming a triaxial ellipsoidal shape for the central body, for an asteroid of the size of Didymos, the SRP acceleration exceeds the perturbation due to the quadrupole term of the gravity field expansion (J_2) after about eight asteroid radii for a millimeter-sized particle and 15 radii for a centimeter-sized one. For a millimeter-sized particle, the SRP exceeds even the monopole term of the gravity attraction after about 140 asteroid radii (for a centimeter-sized particle, the limit is around 450 Didymos radii).

As described in Section 2.2, in order to perform a realistic test of the SRP effects, we have taken into account the changes in the cross section of a particle due to its irregular shape and rotation state. Namely, we integrated the same set of initial conditions of 400 test particles, 5 cm in size, assuming both a spherical and an ellipsoidal shape. The triaxial ellipsoidal particles were chosen with axis ratios $b/a = 0.94$ and $c/a = 0.92$, keeping the same volume as in the spherical case. In the latter case, both a regular rotation around the shortest axis, with a period of 30 s, and a random tumbling were simulated. While clearly limited in scope, the choice of this very specific size for the investigated particles (here and in the following sections) was motivated by a number of reasons. First, we wanted to analyze a size range that would be affected by the SRP but not in an extreme way (such is the case for millimeter and submillimeter particles), and, still, we wanted to consider a size range that would be well populated in a realistic ejecta size distribution. Moreover, the centimeter-sized particles are prone to be ejected with initial velocities in the interesting range below the escape velocity but enough to inject them into orbital trajectories. Given the large uncertainty on the expected rotation state of the ejecta fragments, the 30 s rotation period was adopted as an arbitrary test value to simulate a possibly intermediate situation between the fast tumbling of the random orientation and the fixed value of the aspect area used in the spherical case. As mentioned above, in these sets of simulations, all particles were ejected with a velocity of $\sim$7 cm s^{-1}.

For each of the three cases, 400 test particles were integrated (1200 in total), and all of them ended up colliding with either one of the asteroids within at most 80 days. Figure 3 shows the impact epoch distribution for the three investigated populations.

The median impact time is 21.09 days (mean $= 20.13 \pm 7.86$ days) for the spherical population with 83% of impacts against Didymos and 17% against Dimorphos, 20.25 days (mean $= 19.83 \pm 7.68$ days) for the ellipsoidal population with random rotation with 86% of impacts against Didymos and 14% against Dimorphos, and 20.49 days (mean $= 20.63 \pm 8.23$ days) for the ellipsoidal population with regular rotation with 88% of impacts against Didymos and 12% against Dimorphos.

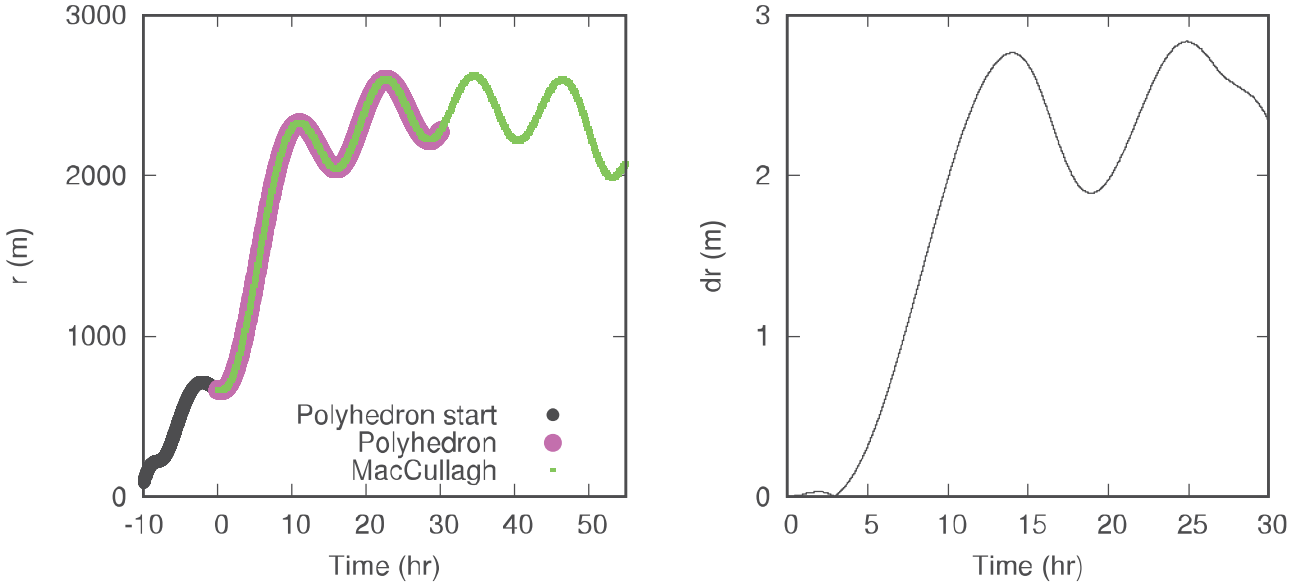

Figure 2. Comparison between the full polyhedron approach and the patched polyhedron–MacCullagh approach. In the left panel, we illustrate with a black line the initial evolution with time, just after the ejection from the surface, of the distance from Dimorphos computed with the polyhedron model. The negative time is adopted to mark at time zero the moment of patching. The continuation of the polyhedron solution (magenta line) is then compared with MacCullagh's solution (green line) at subsequent times. The difference between the two solutions is shown in the right panel.

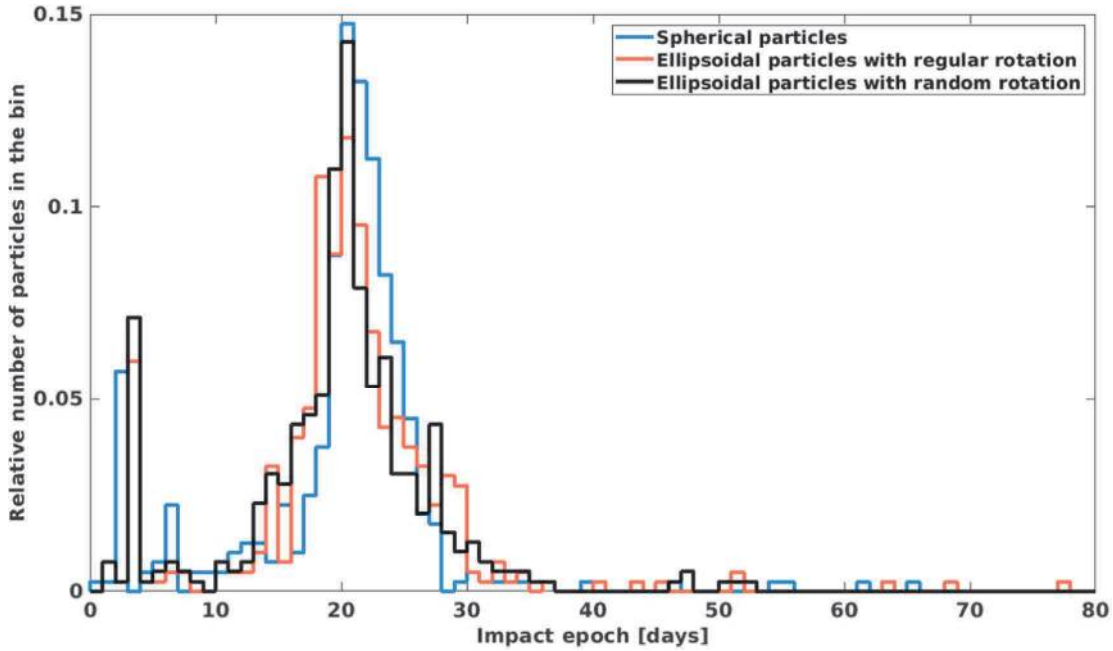

Figure 3. Impact time distribution for the three considered sets of 5 cm–sized particles: spherical (blue line), ellipsoidal with regular rotation (red line), and ellipsoidal with random rotation (black line).

Whereas the median values could suggest an increased lifetime for the case of the spherical particles with respect to the two ellipsoidal cases, it is fair to state that, given the small sample size analyzed, it is not possible at this stage to assert that the observed lifetime ordering would be preserved with a complete ejecta population. Further simulation work is indeed in order to confirm these hypotheses, also taking into account that the dynamics is highly chaotic and strongly influenced by the repeated close approaches with the two massive members of the binary. In the next sections, the chaotic nature of the dynamics will be further investigated.

3. Dynamical Behavior

In this section, the results of a number of tests, performed to study the dynamics of the ejecta on different timescales, are shown.

3.1. Modeling the Short-term Ejecta Evolution

As mentioned, the model can simulate both the short- and long-term evolution of the ejecta dynamics. As an example, Figure 4 shows two snapshots of a short movie of the ejecta plume evolution in the first few minutes after the impact. The

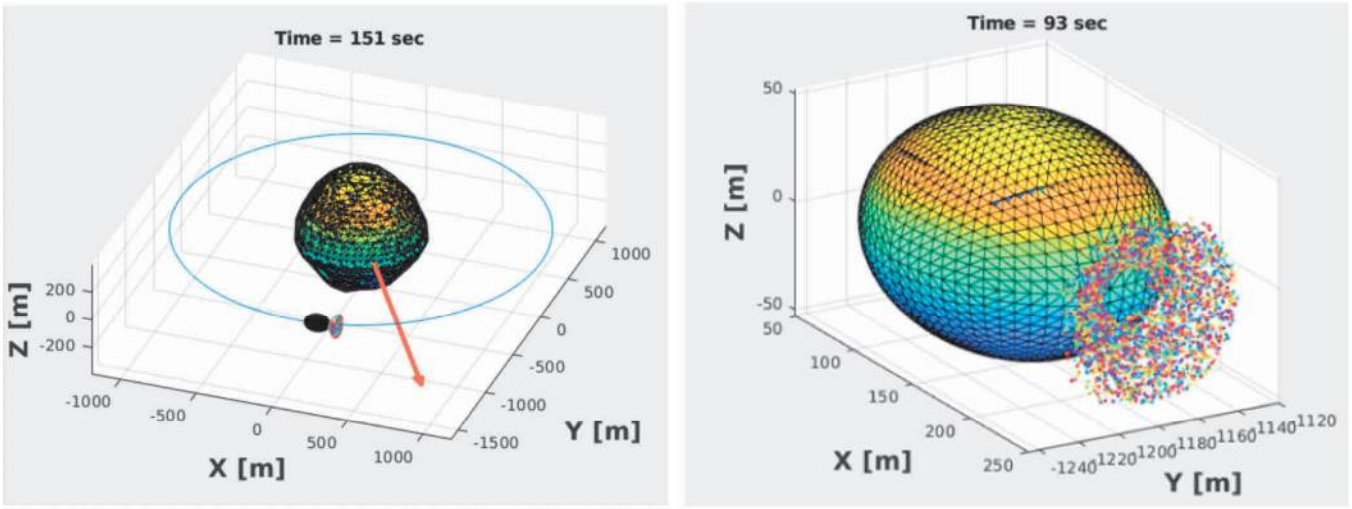

(a) (b)

Figure 4. Left panel: snapshot of a simulation showing the initial evolution (151 s after the impact) of a group of 500 particles (∼5 cm in size) with the full dynamical model. The assumed reference frame (nonrotating) is initially oriented along the principal inertia axes of the central body at time zero. The arrow shows the direction to the Sun. Right panel: detail, centered on Dimorphos, from the same simulation as in the left panel (93 s after the impact).

two plots refer to a simulation evolving a batch of 500 identical ellipsoidal particles (with the same axis ratios as detailed in Section 2.5.2), randomly rotating, ejected with ejection velocities between 5 and 20 cm s^{-1} following the distribution shown in Figure 1. We note that, particularly in these initial phases of the evolution, the ejecta plume is strongly influenced by the ΔV imparted to the particles by the impact. As is well known, very small particles (submillimeter- and millimeter-sized) tend to escape very quickly due to both the imparted ΔV and the SRP effect that tends to quickly become dominant for these kinds of ejecta, even in the proximity of the small central body.

Due to the above caveats, this limited simulation will be repeated with a much larger number of particles to help in the interpretation of the LICIACube images once a reliable set of initial conditions (mainly the initial ΔV) from an impact simulation is available. In particular, coupled with an ongoing analysis of the expected radiance, the simulated evolution of millions of particles (made possible by our fast model) will allow the comparison of the plumes expected for different types of impacted bodies (i.e., different object composition).

It is also worth stressing that, as described in Fahnestock et al. (2022), in the very first phase of the evolution (i.e., in the interval of time encompassed by the LICIACube images), the main perturbations to be considered are the gravity attraction by Dimorphos and Didymos and the SRP with a simplified model (i.e., the SRP effects on ellipsoidal-shaped particles are not relevant in this short time frame). As mentioned, in the current version of the model, collisions between ejecta particles are disregarded. It is also worth noting that, for the global simulation, until a reliable shape model of Dimorphos is available, a simplified gravity field from the analytical ellipsoidal model is well suited to produce the required output. Once a more refined shape model of Dimorphos is available (thanks to the DART and LICIACube images), the simulations will be repeated with the polyhedron model for the primary gravity field.

3.2. Stable Orbits in the Binary Environment

The environment of Didymos and Dimorphos is dynamically complex, and strong perturbations act on particles moving in the proximity of the pair. Stable configurations are found in circumbinary and satellite orbits around Didymos. Dimorphos is too small to support long-term stable satellite orbits unless they are located in very peculiar positions. In Figure 5, we show some examples of orbits that have stable behavior over 2 yr of integration. Note that these particles were propagated disregarding the SRP perturbation in order to initially show potentially stable locations under the effect of the gravitational perturbations (e.g., in the case of large boulders for which the nongravitational perturbations are less prominent). The black line is the orbit of Dimorphos around Didymos, and there are both circumbinary orbits beyond the black line and satellite orbits within it. These are potential locations for rings of particles in the binary that may be trapped and survive for a long time interval. If the trajectories are initially inclined, the nodal precession due to the binary perturbations and the solar tide lead to the formation of a belt of fragments rather than rings. This is shown in Figure 6 for two particles started on orbits with an initial inclination of 45°.

So far, we have considered particles for which the radiation pressure is negligible and perturbed only by gravity. If we include radiation pressure, circumbinary orbits are more easily destabilized, since they are farther away in the gravity field of the main body (Didymos; see Section 2.2). In the left panel of Figure 7, we illustrate the evolution of a spherical particle of radius 0.5 m initially coplanar with Didymos and Dimorphos affected by radiation pressure compared to one with the same initial conditions but for which radiation pressure is negligible. The 0.5 m radius particle becomes unstable after about 400 days from the beginning of the simulation and leaves the system. The radiation pressure, even if weak for a 0.5 m particle, is able to perturb the circumbinary orbit enough to cause its destabilization. On the other side, the right panel of Figure 7 shows the case of a satellite orbit around Didymos. For a particle moving in this orbit, the radius must be reduced to 1 cm in order to destabilize its trajectory and cause its impact

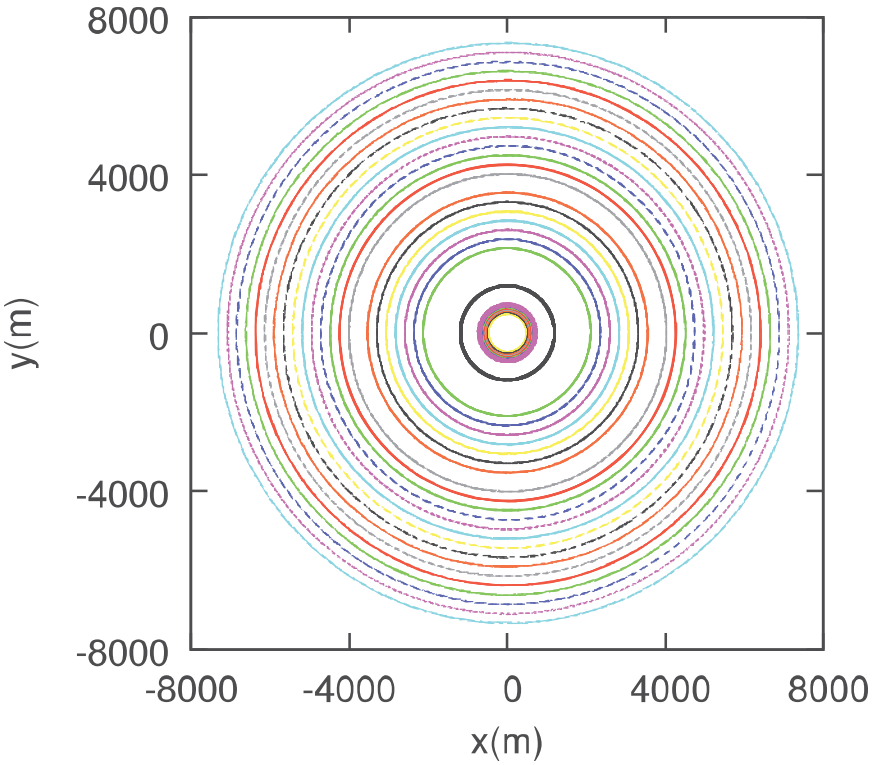

Figure 5. Orbits that are stable over 2 yr of numerical integration. The black line marks the orbit of Dimorphos around Didymos. Note that in these simulations, the SRP is neglected. As mentioned in the text, this accounts for the observed stability.

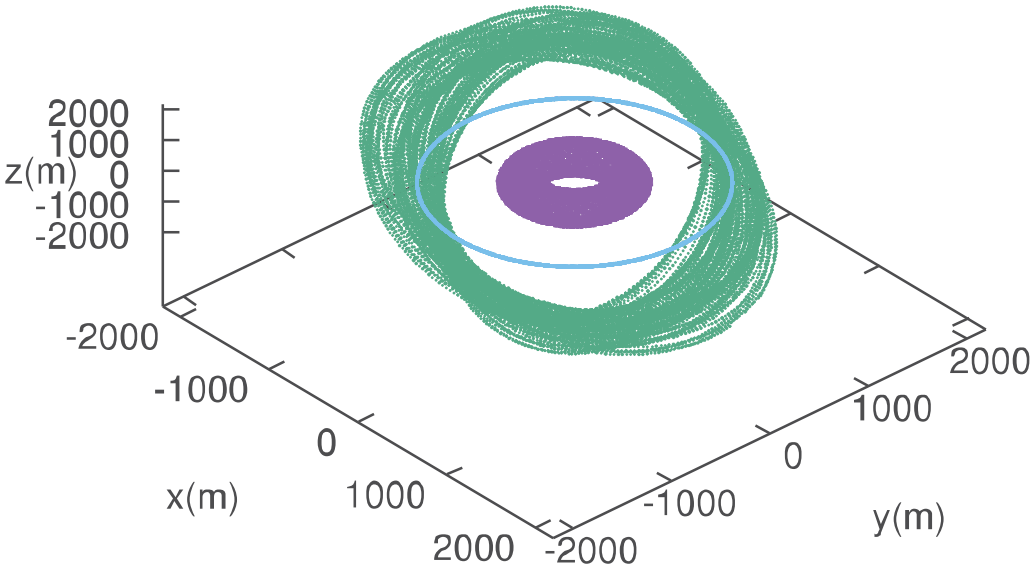

Figure 6. Circumbinary (green line) and circumprimary (purple line) orbits initially started on inclined trajectories ($i = 45°$). Due to the nodal precession, the orbits form a belt around the primary.

on Dimorphos. This outcome suggests that potential rings in the system are more stable in satellite orbits around the primary, while circumbinary rings must be made of big chunks in order to survive over long timescales. The solar tide has negligible effects on the stability of the orbits we have analyzed.

An important question concerns the ejecta from the impact: are the initial velocity and position vectors able to inject some fragments into stable orbits, either circumbinary or satellite, and form rings in the system that might be detected by the Hera mission? The previous orbits have been computed with starting conditions computed from orbital elements, either with respect to the center of mass for circumbinary orbits or with respect to the primary body for satellite orbits, where the eccentricity is initially set to zero. These trajectories are not available to ejecta that evolve from the surface of Dimorphos and, therefore, are set on highly eccentric orbits. Only mutual collisions between the particles in the ejecta could damp the eccentricity and lead the fragments into orbits similar to those shown above. Our model currently does not consider interactions between the ejecta particles (i.e., no collisions are considered). However, as shown, e.g., in Fahnestock et al. (2022), the initial ejecta cloud

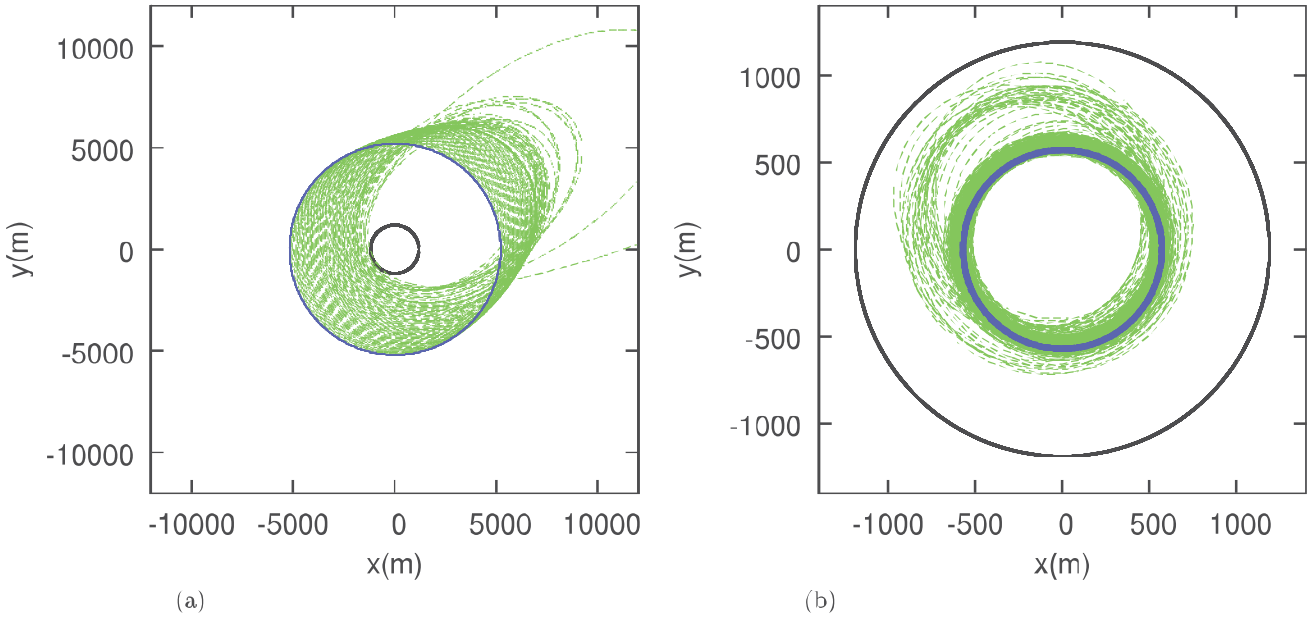

Figure 7. Left panel: comparison between a circumbinary orbit computed without radiation pressure (blue line) and one where radiation pressure is included and computed for a 50 cm radius particle (green line). The black line marks the orbit of Dimorphos around Didymos. Right panel: comparison between a satellite orbit computed without radiation pressure (blue line) and one where radiation pressure is included and computed for a particle having a radius of 1 cm (green line). The black line marks the orbit of Dimorphos around Didymos.

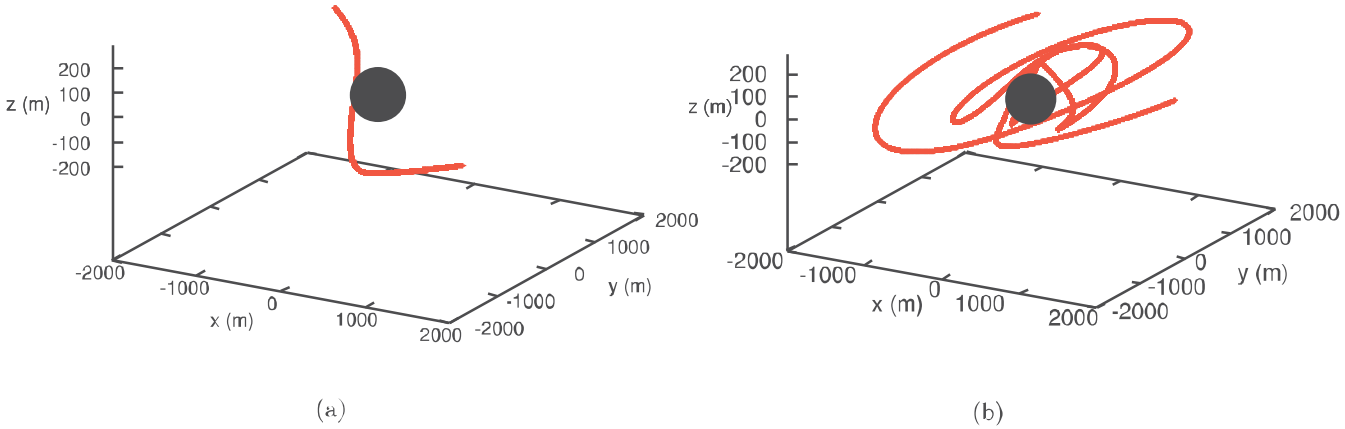

Figure 8. Trajectory of a fragment during a simple close approach to Dimorphos (left panel) and a more complex one characterized by a temporary capture around the asteroid (right panel).

is quickly dispersed to the point that mutual collisions between the particles, already after a few minutes from the DART impact epoch, are not able to cause significant alterations in the orbital evolution.

The next step is then to look for stable orbits among those that are produced by the impact, if they exist, and see if they can form a ring that might be observed by Hera.

3.3. The Chaotic Nature of the Ejecta Trajectories

Once ejected from the surface of Dimorphos, the fragments of the impact end up in trajectories that evolve around the barycenter of the system. The orbital evolution is mostly chaotic due to the binary nature of the dynamical environment. While orbiting around the barycenter, each fragment experiences repeated close encounters with Didymos that gravitationally alter its trajectory with impulsive changes. The new orbit is different from the old one, and these frequent encounters give origin to a chaotic evolution. A slight change in the orbital parameters when the fragment enters the influence sphere of Dimorphos is amplified at the next encounter, and so on.

In Figure 8, we show two examples of close encounters of an ejecta particle with Dimorphos significantly altering its trajectory. The first depicted encounter is a simple hyperbolic approach (left panel), while the second one (right panel) is more complex. A few revolutions around Dimorphos are completed before the fragment departs from the companion asteroid. This chaotic behavior suggests that ejecta from the impact do not have easy access to stable satellite orbits around Didymos.

3.4. The Search for Long-surviving Particles among Ejecta

An interesting question is the possibility of having ejected particles that could enter almost stable orbits and remain in the binary system for comparatively long time spans. Besides the theoretical interest, this is relevant because these particles may

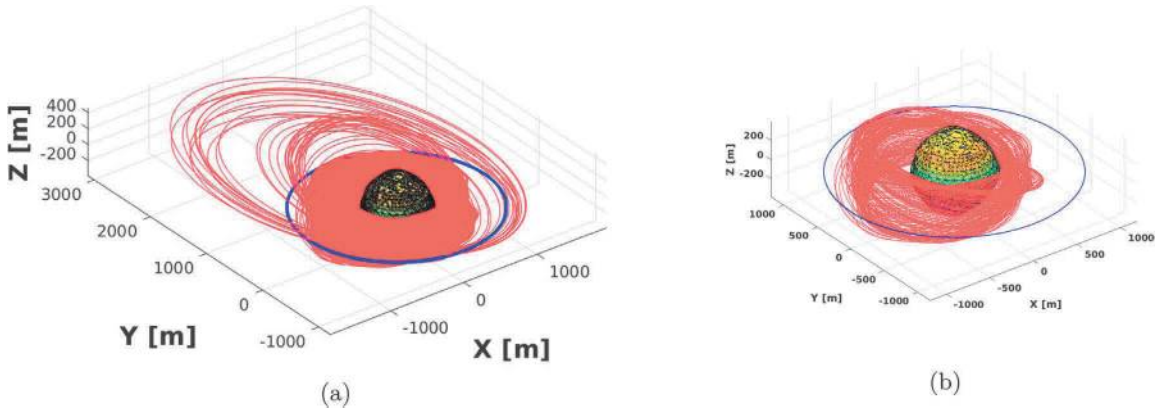

Figure 9. Left panel: full trajectory of the longest-living particle. Right panel: detail of the final orbits from the left panel. The blue circle represents the orbit of Dimorphos around Didymos.

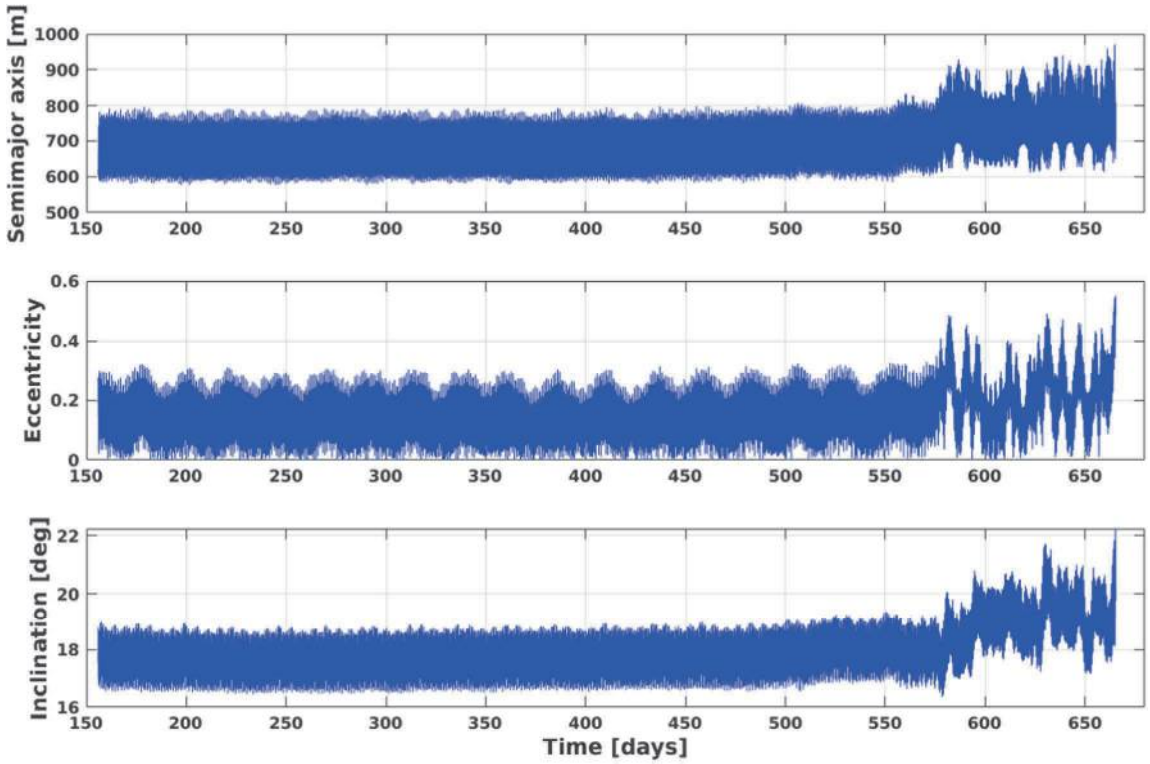

Figure 10. Semimajor axis (top panel), eccentricity (middle panel), and equatorial inclination (bottom panel) of the trajectory shown in Figure 9.

represent a hazard for the Hera probe during its investigations approximately 4 yr after the DART impact. In addition, it would also be interesting to see if these kinds of impact particles can generate a temporary ring around either one of the asteroids. Important questions concern the shape of this putative ring, since the dynamics of the system is very complex, and also for how long it could survive before its dispersal due to the escape of debris from the system or its impact on the asteroid pair. To investigate the long-term stability of ejecta, 500 particles were integrated with a time horizon exceeding 5 yr in order to encompass the Hera arrival delay. All of the considered particles were ellipsoids, with a longest axis of about 5 cm (as defined in Section 2.5.2).

The ellipsoids were assumed to be randomly rotating. As before, the initial Cartesian position and the direction of the ejection velocities were taken from the simulations provided by S. Raducan (Raducan et al. 2019), and the corresponding modulus of the ejection velocities was rescaled to about 7 cm s^{-1}.

The left panel of Figure 9 shows the full trajectory of the longest-living particle found within the sample. The particle is initially ejected in a highly eccentric orbit centered on the barycenter of the system whose eccentricity is also enhanced by the SRP. Later on (see the right panel of Figure 9), it undergoes many close approaches with Dimorphos and is captured in an almost circular, moderately inclined orbit inside the orbit of the satellite asteroid.

The barycentric orbital elements during the stable period are shown in Figure 10. The long quasiperiodic evolution might be related to a 2:1 spin–orbit resonance between the rotation period of Didymos and the orbital period of the particle, which is located around 630 m from the center of Didymos. However, it is expected to be very weak due to the almost spherical shape of Didymos. The stability might also be due to a 1:2 mean-

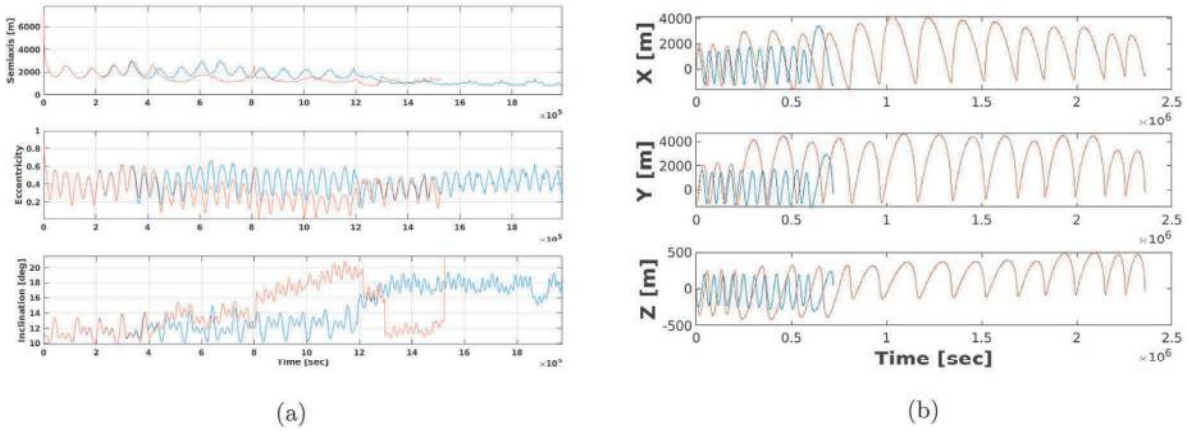

Figure 11. Left panel: orbital elements of the particle of Figure 9 (blue line) compared with the elements of a cloned particle where the *Y*-coordinate was changed by 5 cm with respect to the particle of Figure 9. Right panel: time evolution of the Cartesian coordinates of the trajectory depicted in Figure 9 (orange line) compared to the cloned particle with a ΔV of 0.87 cm s ^{1} (blue line).

motion resonance with the orbit of Dimorphos, which is located about 750 m from the center of Didymos. This quiet period is interrupted after about 400 days by a sequence of close encounters with Dimorphos, and the particle finally impacts on Didymos after 665 days. We note that, while not exactly equal to the interval of time separating the DART impact from the predicted arrival time of Hera at the Didymos system, 665 days can be considered a time span of the order of the DART–Hera delay interval; i.e., finding particles that survive for ∼2 yr is a clear hint that, from a dynamical point of view, long-lived orbits are possible.

To verify the possibility of finding particles lasting even longer, the neighborhood of the initial conditions leading to the long-lasting particle of Figure 9 was explored by propagating 600 clones of that object obtained by changing one of the initial Cartesian coordinates at steps of 1 cm.

None of the cloned particles lasted for a time comparable to the original particle, and their orbits quickly diverged from the one described in Figure 9. As an example, in the left panel of Figure 11, the comparison of the orbital elements of two particles identical to the long-lasting one previously described a part from a deviation of 5 cm in the *Y* Cartesian coordinate. The trajectories of the two bodies begin to diverge after about 5 days, and the clone does not have a chance to be injected into an orbit internal to that of Dimorphos, but it impacts on it after about 20 days.

Similar results were obtained by changing the initial ejection velocity vector. Also in this case, the extreme sensitivity of the results on the initial conditions is shown in the case illustrated in the right panel of Figure 11. A change of 0.87 cm s^{-1} on the magnitude of the initial velocity vector leads to two trajectories that, after a short period where they almost superimpose, quickly diverge.

These tests confirm the chaotic nature of the particle trajectories and also suggest that among all fragments, a fraction may last until the arrival of Hera, since their chaotic evolution is slower than most of the ejecta, and they could form a tiny ring around Didymos. A large sample of particles should be numerically integrated to estimate the amount of dust following the slow evolution path and surviving for at least 2 yr. This approach would also allow us to map the set of initial conditions leading to the long-surviving paths. It is indeed a very complex task, since different combinations of initial position, initial velocity, size, and particle rotation rate might lead to the same (or different) path, and a detailed exploration would require a full sampling of all of these parameters.

3.5. Effect of Ejecta Reimpacts

To study the possible effects of the reimpact of the ejected particles against either one of the two asteroids (after a variable number of revolutions around the two bodies), we studied the evolution of 400 particles. Since we are interested in evaluating the importance of these secondary impact events on the overall dynamics of the binary system in this set of simulations, we considered somehow larger ejecta with respect to the previous simulations. The 400 particles are now randomly rotating ellipsoidal particles of about 10 cm in size, with the axis ratios $b/a = 0.77$ and $c/a = 0.69$. Once more, the ejection velocity was set to 7 cm s^{-1} for all 400 particles, since we are interested in particles that can remain trapped within the binary system. Out of the 400 particles considered for this specific study, 37% impacted against Dimorphos, while 63% ended up against Didymos. The left panel of Figure 12 shows the distribution of the impact velocities for all of the investigated particles, while the right panel shows the epoch of the reimpact events.

The median value of the reimpact velocities of the ejecta particles is 55.93 cm s^{-1} against Didymos and 9.88 cm s^{-1} against Dimorphos. The low velocity values for the reimpact against Dimorphos are due to particles that are almost corotating with the small body reimpacting within shorter time spans after the ejection, while the higher values recorded for Didymos are related to particles that enter into unstable orbits around the system center of mass and finally impact the larger body during a pericenter passage.

It is interesting to note that the distribution of impact velocities shown in Figure 12 is compatible with the one shown in Figure 2 of Yu & Michel (2018) for both Didymos and Dimorphos impacts. On the other hand, it is worth noting that in our case, the spread in the impact velocities is due only to the dynamical evolution of the ejecta particles and is not related to the ejection velocity (as is depicted in Figure 2 of Yu & Michel 2018), since all of our test particles are ejected with the same initial velocity (in magnitude).

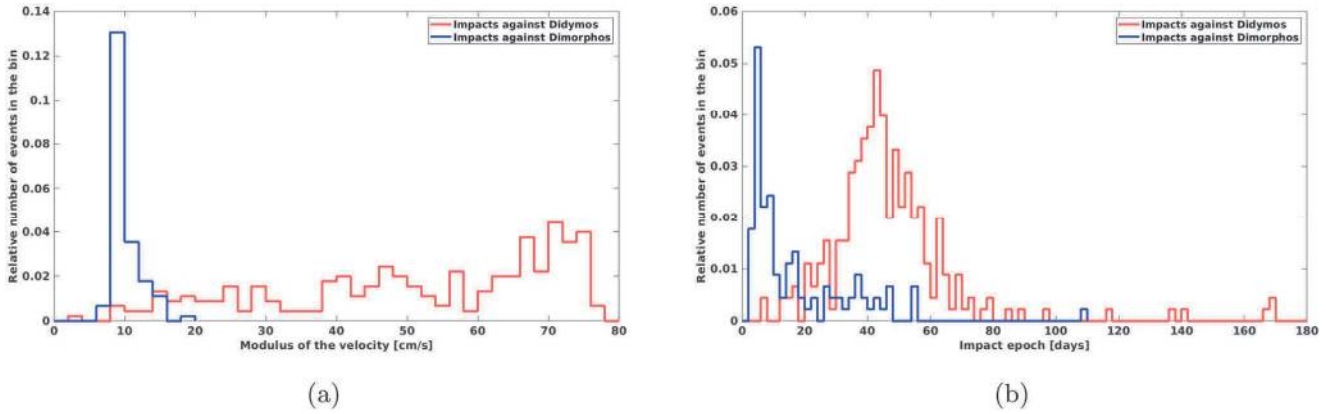

Figure 12. Left panel: distribution of the impact velocities for the ejecta particles reimpacting either against Dimorphos (blue line) or against Didymos (red line). Right panel: distribution of the epochs of impact for the ejecta particles reimpacting either against Dimorphos (blue line) or against Didymos (red line).

It is interesting to evaluate the possible effect of these reimpacting particles on the rotational dynamics of the two asteroids. We remember that the specific angular momentum of a particle is defined by

$$\bar{h} = \frac{\bar{L}}{m} = \bar{r} \times \bar{v}, \tag{5}$$

where $\bar{L}$ is the angular momentum, m is the mass of the impacting particle, $\bar{r}$ is the position vector of the impact location, and $\bar{v}$ is the vector of the impact velocity. The specific angular momentum of a rotating spherical body is given by

$$h_{\rm rot} = \frac{2}{5} R^2 \omega, \tag{6}$$

where R is the body radius, and ω is the rotation frequency. Assuming a rotation period of 2.2593 hr for Didymos and 11.9 hr for Dimorphos, from Equation (6), the modulus of the specific angular momentum of Didymos is $h_{\rm rot}(\text{Didymos}) = 1.88 \times 10^6$ cm^2 s^{-1}, while the one for Dimorphos is $h_{\rm rot}(\text{Dimorphos}) = 4221$ cm^2 s^{-1}.

Computing the average specific momentum for the reimpacting ejecta particles by means of Equation (5), the following values are obtained:

1. 1.59×10^6 cm^2 s^{-1} for impacts against Didymos and
2. 7445 cm^2 s^{-1} for impacts against Dimorphos.

In considering the above "specific" values, it must be taken into account that the mass ratio between an ∼10 cm reimpacting particle and the two asteroids is of the order of 2×10^{-12} for Didymos and 2×10^{-10} for Dimorphos. Hence, it turns out that single impacts of centimeter-sized particles cannot significantly influence the current rotation state of either body. Nonetheless, from the above values, given a proper estimate of the total ejecta mass, it could be possible to derive at least upper limits for the total angular momentum transferred from the reimpacting particles onto the two asteroids. Thus, ultimately, it could be possible to derive an estimate of the change (if any) in the rotation period of the two bodies due to the reimpacting particles' momentum. This computation will be undertaken in future work once a reliable estimate of the total reimpacting mass (starting from impact simulations) is available. Finally, it is worth stressing that these secondary impacts can raise small ejecta particles from the surface of the two bodies, thus possibly contributing to the creation of a dusty environment in the binary system.

4. Discussion and Conclusions

A comprehensive numerical model for the dynamics of the ejecta from the DART impact has been used to explore the plume evolution and the existence of long-lasting trajectories of ejecta fragments that may be detected at the arrival of Hera. In our study, we explored the relevance of the gravitational and nongravitational perturbations and focused on the evolution of the ejecta particles over different timescales, looking for the existence of orbits that are potentially stable over a long timescale in the binary gravity field.

The main conclusions are as follows.

1. Stable orbits over years are found in circumbinary and circumprimary (around Didymos) configurations when the radiation pressure force is negligible. Circumbinary orbits are more sensitive to radiation forces, and even bodies 1 m in size are destabilized on a timescale of a few years when subject to radiation pressure. Circumprimary orbits are more resilient, and particles as big as a few centimeters may be stable over some years. This suggests that potential circumprimary rings should be easier to form and persist.
2. The gravity potential computed with the polyhedron can be effectively substituted with the analytical formulation for nearly ellipsoidal bodies and when the distance from the central body is large enough to minimize the shape effects. A smooth transition between the two models is observed within the model for the simulated ellipsoidal shapes. This allows us to significantly speed up the code and reduce the integration time.
3. In the algorithm for computing the SRP, different models for the rotation of the particles have been tested. Considering fairly regular ellipsoidal particles, the three models give comparable results when looking at the global behavior over long time spans. Whereas some possible systematic effects are observed in the small sample considered when assuming ellipsoidal versus spherical particles, more work is definitely needed on a much larger population to confirm this conclusion.
4. Impact points in the vicinity of the nominal location (within about 10° in latitude and longitude) lead to quite

similar ejecta evolution over a long timescale. On the other hand, as described in Yu & Michel (2018), impacts in the northern and southern regions appear to lead to more long-lived particles (perhaps related to the higher inclination of the ejecta orbits).

5. In our simulations, we found a number of particles ejected with velocities around 10 cm s^{-1} and between 5 and 10 cm in size that can survive for time spans of a few years. This time interval is comparable with the Hera arrival time; hence, there is the possibility that Hera will find DART ejecta particles still in orbit in the system. Most of these low initial velocity, centimeter-sized ejecta particles end up impacting one of the two main bodies in the system.
6. The dynamics of the particles appears extremely chaotic due to the repeated close encounters with either one of the asteroids but, in particular, with Dimorphos at the beginning of their evolution. Very small differences in the initial conditions (either position or velocity vectors) lead to completely different evolutions. This poses some caveats on several aspects of the medium–long-term ejecta simulations. For example, the accuracy of the initial conditions and the modeling of different perturbations has to face the fact that a few centimeters of initial difference in position (or, conversely, in the close approach coordinates) can account for a totally different orbital evolution. Thus, the global properties of the ejecta population over a medium–long time span should be studied by simulating large numbers of test particles.
7. The effect of the ejecta particles reimpacting against the two asteroids after a variable time span can be estimated. Particles ending against Dimorphos and Didymos display clearly different impact velocities. Despite the small addition to the overall angular momentum of the two asteroids of single events, multiple impacts of larger particles (above 10 cm in size) could, in principle, produce a noticeable effect on the rotation state of the asteroids. This aspect is being further analyzed to evaluate the expected changes in the binary dynamics related to the reimpacting particles and the possibility of detection by Hera.

Future work will concentrate on evolving a large number of ejecta particles from different impact simulations (e.g., different ejecta velocities, particle sizes and shapes, etc.) to further evaluate the global midterm evolution of the plume up to the Hera arrival time. The chaotic behavior will be further explored with a detailed orbital elements analysis of the surviving particles to possibly identify regions of stability in the phase space. Finally, the effects of the secondary impacts on the possible creation of a dynamic dusty environment within the binary system will be investigated.

A.R. and the whole LICIACube team acknowledge financial support from Agenzia Spaziale Italiana (ASI, contract No. 2019-31-HH.0 CUP F84I190012600). The authors wish to thank S. Raducan for providing the ejecta initial conditions used in some of the simulations. The authors wish to thank the two anonymous reviewers whose constructive comments helped to improve the paper. The LICIACube Team includes M. Amoroso, I. Bertini, A. Capannolo, B. Cotugno, G. Cremonese, M. Dall'Ora, J. D. P. Deshpariya, V. Di Tana, I. Gai, G. Impresario, M. Lavagna, P. H. Hasselmann, A. Meneghin, F. Miglioretti, D. Modenini, P. Palumbo, D. Perna, S. Pirrotta, G. Poggiali, E. Simioni, S. Simonetti, P. Tortora, M. Zannoni, and G. Zanotti.

ORCID iDs

Alessandro Rossi https://orcid.org/0000-0001-9311-2869
Francesco Marzari https://orcid.org/0000-0003-0724-9987
John Robert Brucato https://orcid.org/0000-0002-4738-5521
Vincenzo Della Corte https://orcid.org/0000-0001-6461-5803
Elisabetta Dotto https://orcid.org/0000-0002-9335-1656
Simone Ieva https://orcid.org/0000-0001-8694-9038
Stavro Lambrov Ivanovski https://orcid.org/0000-0002-8068-7695
Alice Lucchetti https://orcid.org/0000-0001-7413-3058
Elena Mazzotta Epifani https://orcid.org/0000-0003-1412-0946
Maurizio Pajola https://orcid.org/0000-0002-3144-1277
Giovanni Poggiali https://orcid.org/0000-0002-3239-1697
Angelo Zinzi https://orcid.org/0000-0001-5263-5348

References

Braga-Ribas, F., Sicardy, B., Ortiz, J. L., et al. 2014, Natur, 508, 72
Burns, J. A., Lamy, P. L., & Soter, S. 1979, Icar, 40, 1
Dotto, E., Della Corte, V., Amoroso, M., et al. 2021, P&SS, 199, 105185
Everhart, E. 1985, in An Efficient Integrator that Uses Gauss-Radau Spacings, ed. A. Carusi & G. B. Valsecchi (Dordrecht: Springer), 185
Fahnestock, E., Cheng, A., Ivanovski, S., et al. 2022, PSJ, submitted
Giblin, I., Davis, D. R., & Ryan, E. V. 2004, Icar, 171, 487
Marzari, F. 2020, A&A, 643, A67
Michel, P., Kueppers, M., & Fitzsimmons, A. 2022, PSJ, submitted
Milani, A., Nobili, A., & Farinella, P. 1987, Non-gravitional Perturbations and Satellite Geodesy (Bristol: Hilger)
Murray, C. D., & Dermott, S. F. 2000, Solar System Dynamics (Cambridge: Cambridge Univ. Press)
Ortiz, J. L., Duffard, R., Pinilla-Alonso, N., et al. 2015, EPSC, EPSC2015–230
Ortiz, J. L., Santos-Sanz, P., Sicardy, B., et al. 2017, Natur, 550, 219
Raducan, S., Davison, T., & Collins, G. 2021, Icar, 374, 114793
Raducan, S., Davison, T., Luther, R., & Collins, G. S. 2019, Icar, 329, 282
Raducan, S., Jutzi, M., Davison, T., et al. 2022, IJIE, 162, 104147
Rivkin, A. S., Chabot, N. L., Stickle, A. M., et al. 2021, PSJ, 2, 173
Rossi, A., & Fulchignoni, M. 2007, AdSpR, 40, 173
Rossi, A., Marzari, F., & Farinella, P. 1999, EP&S, 51, 1173
Ruprecht, J. D., Bosh, A. S., Person, M. J., et al. 2015, Icar, 252, 271
Stickle, A., Syal, M., Cheng, A., et al. 2020, Icar, 338, 113446
Werner, R. A. 1994, CeMDA, 59, 253
Werner, R. A., & Scheeres, D. J. 1997, CeMDA, 65, 313
Yu, Y., & Michel, P. 2018, Icar, 312, 128
Yu, Y., Michel, P., Schwartz, S. R., Naidu, S. P., & Benner, L. A. M. 2017, Icar, 282, 313
Zhang, Y., Jutzi, M., Michel, P., Raducan, S. D., & Arakawa, M. 2021, EPSC, EPSC2021–704